// Lawrence Berkeley National Laboratory
LBL Publications

Title
Upgrade to the SHARP EUV mask microscope

Permalink
https://escholarship.org/uc/item/9vh7g4rm

Authors
Benk, Markus
Chao, Weilun
Miyakawa, Ryan
et al.

Publication Date
2019-03-26

DOI
10.1117/12.2516387

Peer reviewed

eScholarship.org Powered by the California Digital Library
University of California

Upgrade to the SHARP EUV mask microscope

Markus Benk*, Weilun Chao, Ryan Miyakawa, Kenneth Goldberg, Patrick Naulleau
Center for X-ray Optics, Lawrence Berkeley National Laboratory,
1 Cyclotron Road, Berkeley, CA 94720

ABSTRACT

The Sharp High-NA Actinic Reticle review Project (SHARP) is a synchrotron-based, extreme ultraviolet (EUV) microscope dedicated to photomask research. A potential upgrade to the SHARP microscope is presented. The upgrade includes changing the light path in the instrument from its current off-axis configuration to an on-axis configuration. This change allows for an increased working distance of 2.5 mm or more. A central obscuration, added to the zoneplate aperture, blocks stray light from reaching the central part of the image, thus improving the image contrast. The imaging performance of the two configurations is evaluated by means of ray tracing.

1. INTRODUCTION

The SHARP microscope[1] is the successor to the Berkeley Actinic Inspection Tool[2] (AIT). Like its predecessor, SHARP uses zoneplate lenses in an off-axis configuration as imaging optics. The tool is equipped with a variety of user-selectable zoneplates. The standard zoneplates are designed to match the imaging conditions in EUV scanners in terms of chief-ray angle (CRA) and mask-side numerical aperture. This includes zoneplates matching the mask side NA of the NXE:3300 scanner[3] and zoneplates for to emulation of high-NA anamorphic imaging.[4,5] The illuminator[6] in SHARP synthesizes arbitrary source-angular spectra and readily emulates the illumination conditions in EUV scanners, including freeform SMO sources.

Figure 1 illustrates the light path in the instrument. The illustration is not to scale. The low-divergence synchrotron beam at 13.5-nm wavelength is focused on a flat turning mirror M_A. The condenser mirror in the illuminator images the beamline intermediate focus onto the photomask in critical illumination. Mirror M_A is a MEMS-driven 2D-scanner mirror. The pupil fill is generated scanning the beam across the aperture of the condenser mirror. The zoneplate images the field of view (FOV) at the photomask onto a CCD detector. The center of the image at the CCD detector is vertically above the center of the field of view. The vertical axis through the center of the object plane and the center of the image plane does not pass through the zoneplate. The zoneplate is “off-axis.” The off-axis zoneplate can be viewed as an off-center section of a larger zoneplate with closed circular zones, centered on the vertical axis. The larger zoneplate is referred to as the parent zoneplate. Figure 2 shows the aperture of the off-axis zoneplate and the illumination window with respect to the parent-zoneplate. The illumination window is an opening in the opaque zoneplate membrane. It allows for the light from the illuminator to reach the photomask. To avoid vignetting across the FOV, the illumination window is larger than the zoneplate aperture. The part of the membrane that separates the zoneplate aperture from the illumination window is referred to as the divider.

The purpose of the off-axis configuration is to separate the first diffraction order of the zoneplate from the zero order. Figure 1 (center) shows the light path for the two orders. Specularly reflected light from the photomask, passing through the zoneplate in zero order, misses the CCD detector. The divider between the zoneplate aperture and the illumination window is located vertically above the illuminated region on the photomask. The divider is shown in Figure 2. It prevents direct light from the center of the illuminated region on the photomask from reaching the central part of the image plane. The transport of light is limited to the first diffraction order. The divider does not shadow outer regions of the illuminated area. While specularly reflected light cannot reach the detector, diffracted light from the periphery of the illuminated region can reach the detector.

*mpbenk@lbl.gov; phone 1 510 486-5680; fax 1 510 486-4550

A direct path for diffracted light from the sample to the image exists in many zoneplate-based full-field microscopes. Light taking this path is not focused in the image plane and is therefore usually low in intensity. The resulting contrast loss is often negligible. As opposed to many other microscopic samples, photomasks have high-contrast periodic structures. In SHARP, such structures at the periphery of the illuminated area can efficiently scatter light on the detector at a pitch-dependent angle. The scatter has the shape of the illuminator. To eliminate scatter from the central part of the image, the corresponding fraction of the source angular spectrum has to be dark. As a consequence, some patterns have to be image with a modified illuminator on the SHARP microscope that differs from the requested source.

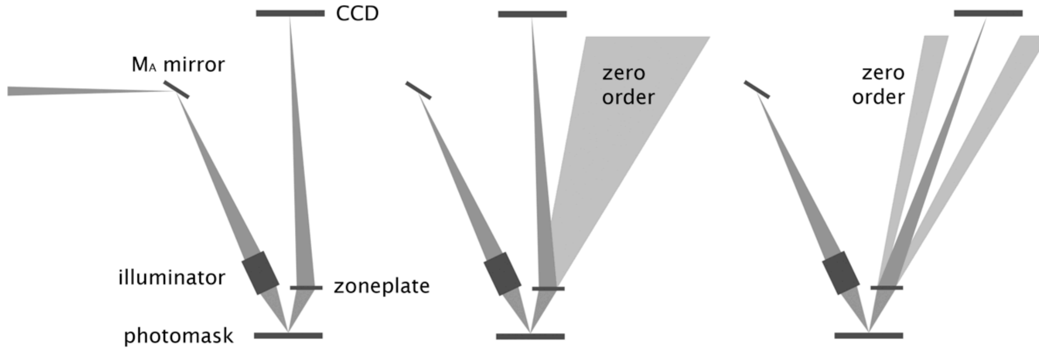

Figure 1. Light pass in the SHARP microscope: (left) overview and naming of the components; (center) first and zero diffraction orders in off-axis configuration; (right) first and zero diffraction orders in on-axis configuration.

As an alternative to an off-axis zoneplate for separating the first and zero diffraction orders, a zoneplate with a central obscuration can be used in an on-axis configuration. We note that the anamorphic imaging optic in the high-NA EUV scanner is expected to also have a central obscuration.[7] In order to accurately emulate imaging in this scanner on the SHARP microscope, a central obscuration needs to be added to the anamorphic zoneplates. With respect to zoneplate-based EUV mask-imaging microscopes, there are advantages and disadvantages to both configurations. However, if the zoneplate is generally required to have a central obscuration in order to mimic future lithography systems, the on-axis configuration is clearly more favorable. A change to an on-axis configuration with centrally obscured zoneplates has to be made for all imaging modes, including 0.33 4xNA.

Figure 1(right) shows the light path for the on-axis configuration. The axis through the center of the object plane and the center of the image plane passes through the zoneplate aperture. The axis is tilted by the CRA with respect to the mask plane, zoneplate aperture and the detector. These components are parallel with each other, both for the off-axis and the on-axis configuration. Figure 1 (right) also shows the light path for the first and zero diffraction orders. The elimination of the central portion of the zero order by the central obscuration is illustrated.

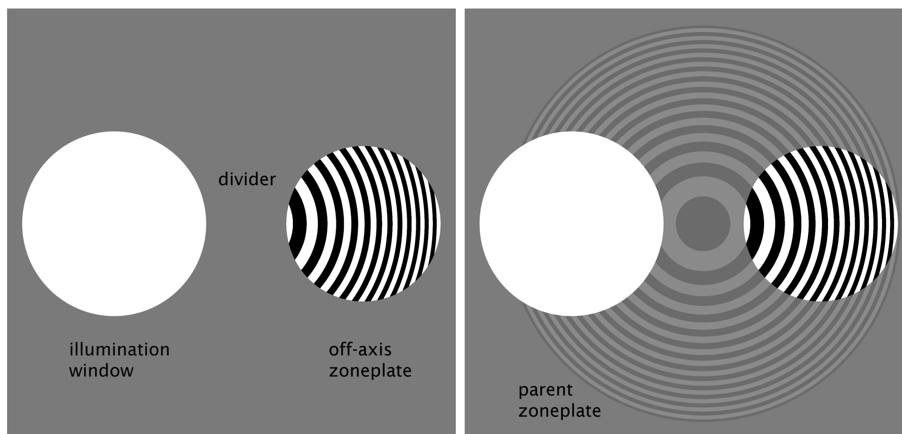

Figure 2. Zoneplate membrane with zoneplate aperture and illumination window: (left) naming of parts; (right) location of the illumination window and zoneplate aperture with respect to the parent zoneplate.

In the current off-axis configuration, the divider blocks direct light from the central part of the illuminated area from reaching the CCD detector. In the on-axis configuration, the central obscuration blocks this light. The radius R of the FOV that is protected from direct light in the image depends on the size of the central obscuration and the size of the illuminated area on the mask:

$$R \approx \mathrm{NA} \cdot s \cdot p - r \tag{1}$$

NA is the mask-side numerical aperture. The relative angular extent of the obscuration is s. The working distance is p and the radius of the illuminated area is r. The situation is similar for the off-axis configuration. The radius of the stop $\mathrm{NA} \cdot s \cdot p$ is replaced with half the width of the divider. The divider has a minimum full width of 18 µm for the 0.33 4xNA zoneplates. The illumination profile in the SHARP microscope is approximately Gaussian. The illumination is mostly uniform over the central 4x4 μm^2 quality region and rolls off from there. At a radius of 15 µm, the intensity is less than 3% for typical illuminator settings. The size of the illuminated region can be reduced at the expense of flux and uniformity in the center. In order to work with a radius of the illuminated area of 15 µm, the radius of the stop should be at least 20 µm to eliminate stray light across the FOV.

Equation 1 shows that for a given NA and angular extent of the stop, the size of the shadowed region is proportional to the working distance. The focal length of a zoneplate is wavelength-dependent. Therefore, monochromatic light is required for zoneplate imaging. The required bandwidth is often lower than the bandwidth of EUV light after multiple reflections on multilayer mirrors. The inverse relative bandwidth $\lambda/\Delta\lambda$ of the light has to be equal to or larger than the number of zones of the zoneplate N:

$$\frac{\lambda}{\Delta\lambda} \geq N \tag{2}$$

For a given numerical aperture the number of zones is proportional to the working distance of the zoneplate:

$$N \approx p \cdot \frac{\mathrm{NA}^2}{\lambda} \tag{3}$$

For an off-axis zoneplate, NA is the numerical aperture of the parent zoneplate, which is approximately NA+CRA.

Table 1 summarizes the size of the stop, or shadow, for different zoneplate apertures and working distances. The size of the shadow, calculated from equation 1, has been verified by means of ray tracing with the exact geometries. For the anamorphic zoneplates the shadow is calculated along the low-NA direction, which is 0.55/8 at the mask side. The off-axis configuration is included for reference. The table also shows the number of zones for each zoneplate, which corresponds to the inverse bandwidth requirement.

Table 1. Size of the shadowed region and number of zones for zoneplates with different NA values and working distances.

	0.33 off-axis	**0.33**	**0.33**	**0.33**		**0.33**		**0.55**	**0.55**	**0.55**
p [mm]	0.5	0.5	1.5	2.5		3		1.5	2.5	3
s (stop)	n/a	0.2	0.2	0.1	0.2	0.1	0.2	0.2	0.2	0.2
shadow [µm]	9	8	25	20	40	25	50	20	35	40
N	1300	250	750	1250		1500		2100	3500	4200

The parent of the 0.33 4xNA zoneplate in the off-axis configuration has about 1300 zones. The half width of the shadowed region is 9 µm. For an on-axis zoneplate at the same working distance, N drops to 250. The radius of the shadow is below 20 µm. It is 8 µm, which is similar to the off-axis configuration. At a working distance of 1.5 mm the shadow has a radius of 25 µm for an obscuration of 20% of the pupil radius. At 2.5-mm working distance, the required 20-µm radius of the shadow can be achieved with an obscuration of 10% of the pupil radius. With a larger obscuration, a

larger FOV can be realized. The FOV further increases for 3-mm working distance. At 2.5-mm working distance *N* is lower than for the current off-axis configuration and at 3-mm working distance *N* is only moderately larger.

With an obscuration of 20% of the pupil radius the anamorphic zoneplates meet the requirement for the radius of the shadow at a working distance of 1.5 mm and above. The size of the obscuration is taken from Reference 7. Due to the higher NA, the number of zones is significantly larger for the anamorphic zoneplates. The corresponding reduced bandwidth can be achieved at the beamline at the expense of flux. $\Delta\lambda$ is proportional to the width of the exit slit of the monochromator. A 3x reduction in bandwidth leads to a 3x reduction in flux.

All of the on-axis zoneplates at 0.33 4xNA from Table 1 can be operated at a bandwidth similar to the current configuration. The throughput of the instrument is not affected for this NA. In order to achieve similar exposure levels with the high-NA anamorphic zoneplates, the exposure time has to be increased to compensate for the reduction in flux at a reduced bandwidth.

The CCD detector that is currently used in the SHARP microscope has a read-out time of approximately 5 seconds, which is significantly larger than the typical 3-s exposure time. Read-out time is a limiting factor in terms of throughput of the microscope. The Detector Group at Lawrence Berkeley National Lab builds a range of detectors for scientific applications in the extreme ultraviolet and soft x-ray spectral range, including active-pixel image sensors (APS). These sensors have virtually no readout time. Using an APS allows for increasing the exposure time by 5 seconds without increasing the total acquisition time of the image. Based on the standard 3-s exposure, the exposure time can be increased by a factor 2.5. The APS are available with a pixel size of 5 µm. The current CCD detector has 13.5-µm pixels. At a magnification of 900, one pixel in the image corresponds to 15 nm on the mask. To match this number for an image sensor with 5-µm pixels, the magnification has to be 333. This lower magnification is beneficial for a configuration with an increased working distance. It partially offsets the increase in image distance and overall height of the microscope.

The blazed grating of the monochromator at the beamline is designed to operate across a range of wavelengths. A multilayer-coated blazed grating[9] can be optimized for 13.5-nm wavelength. For this type of grating the efficiency at the design-wavelength is higher. Replacing the grating of the monochromator allows for a moderate increase in flux at 13.5 nm. The goal in replacing both the image sensor and the grating is to fully compensate for the loss in flux caused by the lower bandwidth requirement at high-NA and preserve the throughput of the microscope.

2. IMAGING PROPERTIES

SHARP is a single-lens imaging system. The field point in the center of the field of view is imaged onto the detector with no aberration. Field-dependent aberrations are present for off-center points, predominately astigmatism. Within the central region, or sweet spot, the aberrations are small compared to diffraction effects. The diffraction-limited sweet spot of the image is rated at 4x4 μm^2. Ray tracing with the software ZEMAX is used to evaluate the imaging characteristics of the on-axis configuration and compare to the current off-axis configuration. Four field points at an offset at the mask of 2 µm in x and y and the central field point are traced. The system is modeled backwards, from the detector to the object plane. Accordingly, in the detector plane the field points have an offset of 2 µm times the magnification.

Figure 3 shows the through-focus spot diagram for the points and the field-curvature plot for the current off-axis configuration. Both plots show the tilted focal plane in SHARP. The field points on the y-axis come in focus at different through-focus steps. All points along the x-axis come in focus at zero defocus. In the field-curvature plot the sagittal surface has a tilt of 6º, which corresponds to the CRA. The tangential surface has a tilt of 18º. The curvature itself is negligible across the field. The tilt is caused by the 6º angle between the chief ray and zoneplate aperture. To eliminate defocus in the ray-tracing data, a 12º tilt is applied to the mask-side plane, which is the image plane in the model. Figure 4 shows the resulting spot diagram and curvature plot. All field points come in focus at zero defocus. The sagittal and tangential surfaces are symmetric with respect to the tilted plane.

The spot diagram of the five points at best focus for the off-axis configuration is presented in Figure 5. The RMS radius of the off-center field points is 17 nm at the mask side. Figure 5 (right) shows the spot diagram in comparison to the Airy disk at a radius of 100 nm.

Ray tracing in the on-axis configuration using the working distance and magnification of the current off-axis configuration produces similar results. The light path on the mask side, which is the high-NA side in the microscope, is identical for both configurations. The different tilt of the chief-ray with respect to the zoneplate aperture and detector plane on the low-NA side has a marginal effect on the tilt of the mask-side focal plane. The spot diagram is similar. Increasing the working distance to 3 mm and reducing the magnification to 333 does not significantly alter the imaging properties of the system. Figure 6 shows the spot diagram at best focus and the field-curvature plot for this configuration. The tilt of the mask-side focal plane is close to 12º. The RMS radius of the off-center field points is 17 nm for this configuration as well. The ray-tracing results suggest that the on-axis configuration has an imaging performance similar to the current off-axis configuration.

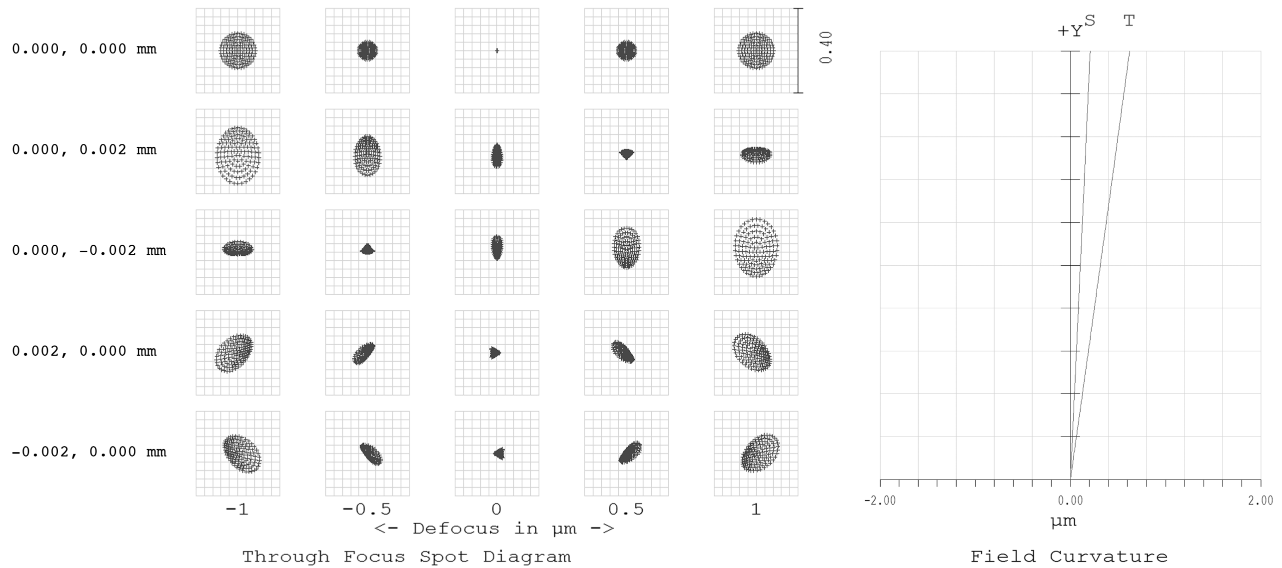

Figure 3. Through-focus spot diagram and field-curvature plot for the off-axis configuration. The mask-side plane is parallel to the zoneplate.

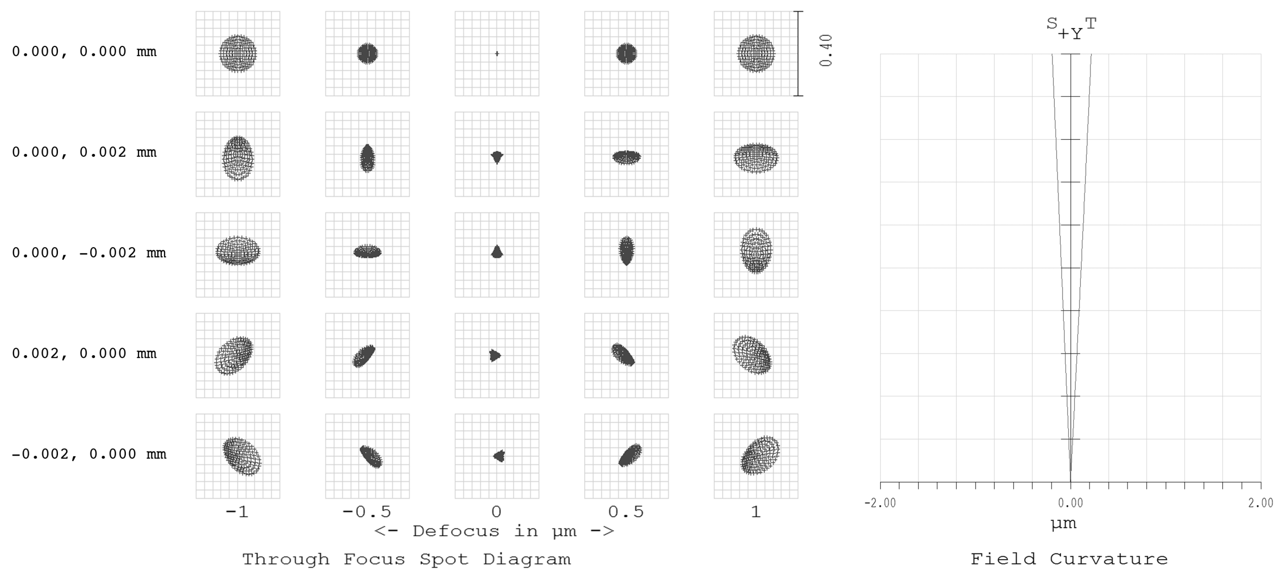

Figure 4. Through-focus spot diagram and field-curvature plot for the off-axis configuration. The mask-side plane is tilted 12º with respect to the zoneplate.

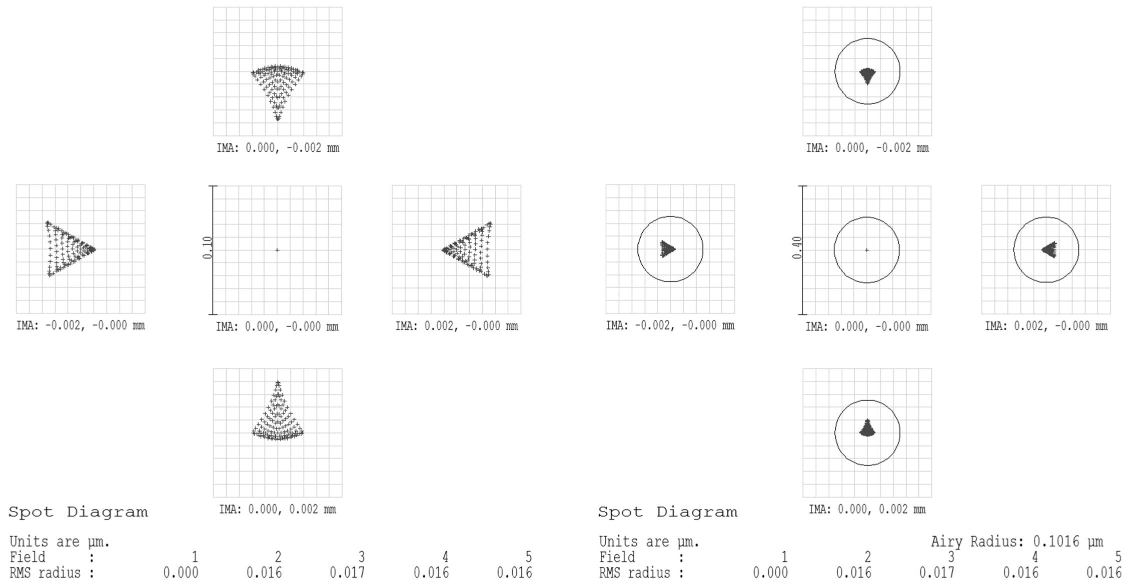

Figure 5. In-focus spot diagram of the central field point and field points 2 µm off center at the mask side for the off-axis configuration: (left) regular spot diagram; (right) spot diagram and Airy disk.

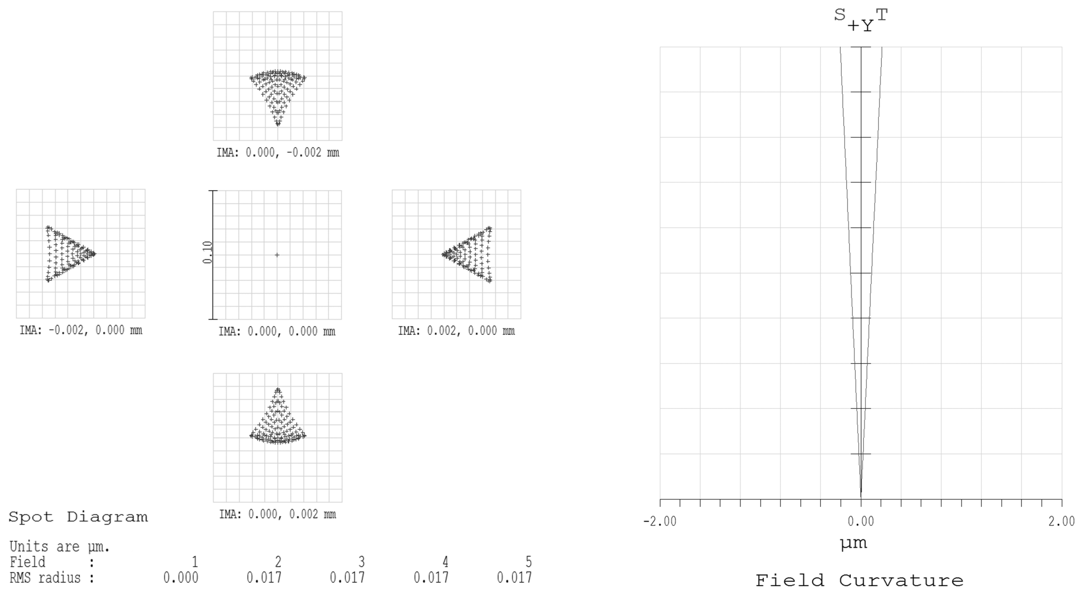

Figure 6. In-focus spot diagram of the central field point and field points 2 µm off center at the mask side for the on-axis configuration at 3-mm working distance and a magnification of 333.

3. SUMMARY

An alternative light path for the SHARP EUV mask microscope has been discussed. Changing the zoneplate lenses from the current off-axis configuration to an on-axis configuration allows for an increased working distance of 2.5 mm and beyond. In the on-axis configuration a central obscuration in the zoneplate aperture is required. The size of the obscuration scales with the working distance. A large obscuration at an increased working distance keeps stray light from reaching the central part of the image, thus improving the image contrast. On-axis zoneplates with increased working distance at 0.33 4xNA can be operated at a spectral bandwidth similar to the bandwidth of the off-axis zoneplates. At an increased working distance, the bandwidth for the high-NA anamorphic zoneplates in the on-axis configuration needs to be three times lower. Replacing the CCD detector with an active-pixel image sensor eliminates the 5-s readout time per image. With this sensor the exposure time can be increased by a factor 2.5 without affecting the total acquisition time of the image. Replacing the grating in the monochromator at the beamline with a multilayer-coated grating increases the flux at 13.5-nm wavelength. Replacing both components is expected to fully compensate for the loss in flux caused by the lower bandwidth requirement at high-NA, thus preserving the throughput of the microscope. The imaging properties of the two configurations are evaluated by means of ray tracing. The results indicate that the imaging performance of the on-axis configuration is similar to the imaging performance of the off-axis configuration.

This work was performed at Lawrence Berkeley National Laboratory with support from Intel through the U.S. Department of Energy under Contract No. DE-AC02-05CH11231. General EUV infrastructure at Lawrence Berkeley National Laboratory is further supported by Intel, Samsung, EUV Tech, Inpria, and JSR through the U.S. Department of Energy under Contract No. DE-AC02-05CH11231.

REFERENCES

[1] K.A. Goldberg, I. Mochi, M. Benk, A. P. Allezy, M. R. Dickinson, et al., "Commissioning an EUV mask microscope for lithography generations reaching 8 nm," Proc. SPIE **8679**, 867919 (2013).

[2] K. A. Goldberg, P. Naulleau, I. Mochi, E. H. Anderson, S. B. Rekawa, C. D. Kemp, R. F. Gunion, H.-S. Han, and S. Huh, "Actinic extreme ultraviolet mask inspection beyond 0.25 numerical aperture," J. Vac. Sci. Technol. B **26**, 2220-4 (2008).

[3] A. Pirati, R. Peters, D. Smith, S. Lok, A. Minnaert, et al., "Performance overview and outlook of EUV lithography systems," Proc. SPIE 9422, 94221P (2015).

[4] M. Benk, A. Wojdyla, W. Chao, F. Salmassi, S. Oh, Y.-G. Wang, R. Miyakawa, P. Naulleau, and K. Goldberg, "Emulation of anamorphic imaging on the SHARP extreme ultraviolet mask microscope," J. Micro. Nanolithogr. MEMS MOEMS **15** (3), 033501 (2016).

[5] V. Wiaux, V. Philipsen, and E. Hendrickx, "Mask 3D effects Experimental Measurements with NA 0.55 Anamorphic Imaging," Proc. SPIE **10809**, 1080913 (2018).

[6] P. P. Naulleau, K. A. Goldberg, P. Batson, J. Bokor, P. Denham, and S. Rekawa, "Fourier-synthesis custom coherence illuminator for extreme ultraviolet microfield lithography," Appl. Opt. **42** (5), 820-826 (2003).

[7] J. van Schoot, K. Troost, F. Bornebroek, R. van Ballegoij, S. Lok, et al., "High-NA EUV lithography enabling Moore's law in the next decade," Proc. SPIE **10450**, 104500U (2017).

[8] K. van Ingen Schenau, G. Bottiglieri, J. van Schoot, J.-T. Neumann, M. Roesch, "Imaging performance of the EUV high NA anamorphic system," Proc. SPIE **9661**, 96610S (2015).

[9] D. L. Voronov, E. M. Gullikson, F. Salmassi, T. Warwick, and H. A. Padmore, "Enhancement of diffraction efficiency via higher-order operation of a multilayer blazed grating," Opt. Lett. **39**, (2014).